Vol. 107: 249–258, 2014
doi: 10.3354/dao02680

DISEASES OF AQUATIC ORGANISMS
Dis Aquat Org

Published January 16

# Fourier-transformed infrared spectroscopy: a tool to identify gross chemical changes from healthy to yellow band disease tissues

**Mayamarú Guerra[1], Maria Antonieta López[1], Ivan Estéves[2], Ainhoa L. Zubillaga[3], Aldo Cróquer[4,*]**

[1]Unidad de Tecnología Laser y Optoelectrónica and [2]Unidad de Geoquímica, Instituto Zuliano de Investigaciones Tecnológicas, Km 15 Carretera Via a La Cañada, Maracaibo 4001, Venezuela

[3]Departamento de Biología de Organismos and [4]Departamento de Estudios Ambientales, Universidad Simón Bolívar, Apdo. 89000, Caracas, Venezuela

ABSTRACT: Yellow band disease (YBD) is a common and wide-spread Caribbean syndrome that affects the genus *Orbicella*, a group of species that constitute the framework of Caribbean coral reefs. Previous studies have shown that the structure and function of bacterial assemblages vary between healthy tissues and YBD lesions; however, how the molecular composition of tissues varies as tissues transition from healthy to YBD has not been determined before. The present study provides the first survey of macromolecules found from healthy (H), apparently healthy (AH), transition (TR) and YBD tissues of *Orbicella faveolata*. For this, we used Fourier-transformed mid-infrared spectroscopy (FTIR) to compare absorption profiles as a proxy for the gross molecular composition of decalcified H, AH and YBD tissues. We found a significantly higher level of infrared absorption for bands assigned to lipids in H tissues compared to YBD tissues, suggesting that lipid compounds are more abundant in compromised tissues in relation to other macromolecules. We also found a lower level of intensity of bands assigned to carbohydrates and proteins in YBD tissues, compared to H and AH tissues. A similar pattern was observed for phospholipidic compounds in relation to fatty acids. This study is the first to show that healthy and YBD-compromised tissues have different infrared absorption profiles, suggesting that alterations in the biochemical composition occur during pathogenesis. Future studies should focus on determining the actual concentration of these compounds in H, AH, TR and YBD tissues and on testing the role of translocation of photoassimilates from H tissues and/or from endolithic algae to YBD tissues.

KEY WORDS: Coral diseases · Yellow band disease · Infrared spectroscopy · Tissue composition



## INTRODUCTION

The Caribbean region is considered a 'hot spot' of coral diseases (Green & Bruckner 2000, Weil 2004) due to the rapid emergence and high virulence of coral reef diseases/syndromes, their widespread geographic distribution, wide host ranges and frequent epizootic events with significant coral mortalities (Sutherland et al. 2004, Weil et al. 2006). Coral diseases or syndromes, along with other unidentified health problems, seem to be challenging coral reef resilience in the Caribbean in different ways (Weil 2004, Weil et al. 2006). Coral diseases compromise the reproductive output of individual colonies (Weil et al. 2009), decrease population numbers of highly susceptible coral species (Bruckner & Bruckner 2006) and reduce coral cover, rendering changes in community structure (Weil 2004) and probably in ecosystem function.

*Corresponding author: croquereef@gmail.com

Among the diseases described from the Caribbean (Green & Bruckner 2000), yellow band (YBD) is arguably the one with the largest detrimental and longest lasting effects for coral reef health in the region (Cróquer et al. 2012). This syndrome tends to be persistent (Bruckner & Bruckner 2006), and it affects all species in the genera *Orbicella and Montastraea* e.g. *O. annularis*, *O. faveolata*, *O. franksi* and *M. cavernosa*), which are the dominant reef-building corals in the region (for specific examples, see Cortés 2003). Furthermore, YBD compromises the fecundity of *M. faveolata* (Weil et al. 2009), produces significant mortality on larger colonies and has contributed to an overall reduction of live coral cover (Bruckner & Bruckner 2006) over the past decades. Combined, these impacts significantly affect the population size of *Orbicella* species, and therefore, it has been hypothesized that YBD alone might reduce reef complexity throughout the Caribbean (Bruckner & Bruckner 2006). While other Caribbean diseases such as white plague, white band, white pox and patchy necrosis may reduce coral cover rapidly, infected hosts often survive from these infections as they show a seasonal pattern that allows lesions to heal. In contrast, YBD progresses at lower rates, but corals seldom recover from infections, hampering the actual chance of survival of infected hosts.

The etiology of YBD has been linked to 4 different strains of *Vibrio* (FGL2A, YBFL3, YB36 and YBM2; Cervino et al. 2004). In addition, recent studies have shown that the transition from healthy to YBD states is characterized by a significant increase in bacterial diversity, particularly Vibrios, and phase shifts in the structure and function of these bacterial assemblages associated with *Orbicella faveolata* (Kimes et al. 2010, Cróquer et al. 2012). YBD has also been shown to affect the immune responses of this species by increasing the activity of small lysozyme-like proteins that are commonly grouped with antibacterial peptides, due to their small size and ability to hydrolyze the β-1,4 glycosidic bond of peptidoglycans in bacterial cell walls (Bachali et al. 2002). Despite YBD representing a major concern to Caribbean coral reefs, the mechanisms implicated in coral tissue mortality still remain in debate and poorly understood (Cróquer et al. 2012), and no comparisons of structural and chemical features of healthy and YBD tissues have ever been made.

According to the coral holobiont hypothesis (Rowan 1998), corals provide a suitable habitat not only for bacterial associates but also for a wide range of microorganisms such as symbiotic algae, viruses and fungi that interact with each other, with the host and with the surrounding environment (Ritchie & Smith 2004, Wegley et al. 2004, Sweet et al. 2011a,b). These microbial associates are spatially structured, with different assemblages thriving in the surface mucus layer (SML), the tissue and the coral skeleton (Sweet et al. 2011b). Each of these habitats provide numerous carbon sources for different microbial guilds that play an important role in nutrient cycling and/or the biogeochemistry of corals (Ferrier-Pagès et al. 1998, 2000, Lesser et al. 2007, Chimetto et al. 2008, Olson et al. 2009, Raina et al. 2009, Kimes et al. 2010). Coral microbial associations are also important for the synthesis and metabolism of a myriad of organic compounds, such as lipids, carbohydrates, organic acids, glycoproteins and more complex polymers, such as enzymes and antibiotic-like compounds (Rohwer & Kelley 2004, Kelman et al. 2006, Ritchie 2006, Nissimov et al. 2009, Shnit-Orland & Kushmaro 2009, Kvennefors et al. 2010), that are essential either for metabolism (Ritchie & Smith 1995, 2004) and/or for various mechanisms of defense (Gochfeld & Aeby 2008).

The chemical composition of the SML and the coral tissues are both susceptible to rapid change due to variations in the contribution of photoassimilates of zooxanthellae, the metabolism of microbial partners and/or the coral host (Rowan et al. 1997, Ritchie & Smith 1995, 2004), for such a physically close assemblage typically shows a high degree of syntropy or co-metabolism. Because the structure and function of the coral-associated microbiota shift from healthy to YBD states (Kimes et al. 2010, Cróquer et al. 2012), it should not be surprising that the chemical properties of the SML and the coral tissues change accordingly with the status of the coral host because the organic by-products of particular metabolic groups of bacteria are often the organic substrates for another (Ritchie & Smith 2004).

The present study aimed to compare the gross chemical composition (i.e. the presence or absence of large families of biomolecules such as carbohydrates, lipids, proteins and nucleic acids) of healthy, apparently healthy, transition and YBD tissues in the reef building coral *Orbicella faveolata* using Fourier-transformed infrared spectroscopy (FTIR; Miller & Dumas 2006). Macromolecules produce specific banding profiles in the infrared spectra or 'fingerprints', which are good estimates of the bulk molecular composition of biological samples (Ami et al. 2004, Barth 2007). These fingerprints are absorption profiles characteristic of each functional group that vibrates at specific bands in the IR spectrum. Fourier-transformed infrared spectroscopy has been widely used to examine numerous types of plant and animal tis-

sues (Wetzel & LeVine 1999, Ami et al. 2004), providing a direct indication of sample biochemistry (Miller & Dumas 2006, Barth 2007). In corals, this technique has been already utilized to describe the bulk composition of macromolecules associated with carbonate skeletons (Farre et al. 2010); however, Fourier-transformed infrared spectroscopy has never been used in the study of coral diseases. Fourier-transformed infrared spectroscopy could be a powerful tool for getting chemical fingerprints of healthy coral tissues for early detection of coral pathology.

## MATERIALS AND METHODS

### Sample collection and coral decalcification

Samples were collected with hammer and chisel from independent colonies with similar diameter (1.5 to 2.0 m) that were located at the same depth (10 m) and separated by at least 5 m to avoid clone mates (ramets). Tissue samples were collected from 7 healthy colonies (H) with no signs of any disease or other stress, 4 apparently healthy colonies (AH), collected from healthy areas of corals with YBD, 4 transition (TR) areas, collected 2 to 3 cm from 4 colonies with YBD lesions, and 4 YBD, collected from another independent set of diseased colonies (YBD; Fig. 1). The samples varied from 3 to 4 cm in diameter. Samples were stored in 96% ethanol solution and decalcified in the laboratory with multiple changes of 10% hydrochloric acid. On completion of decalcification, all samples were rinsed with deionised water and dried at 30°C for 24 h before processing.

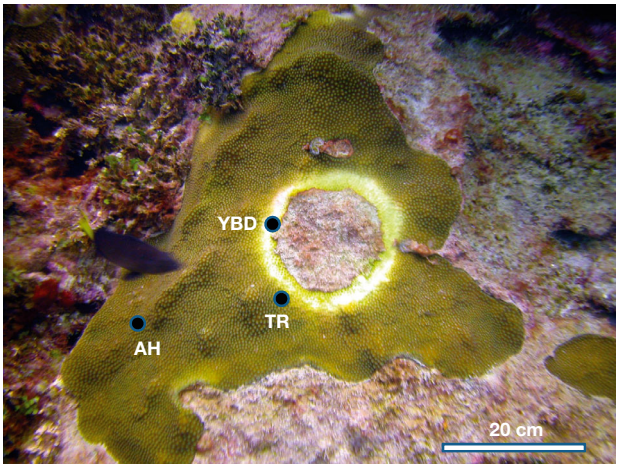


Fig. 1. *Orbicella faveolata*. A colony displaying the classic signs of yellow band disease, and the position of each of the samples collected. AH: apparently healthy; TR: transition; YBD: yellow band disease tissues

### Fourier-transformed mid-infrared spectroscopy (FTIR)

Infrared absorption spectra from 3700 to 550 $cm^{-1}$ were acquired by a Shimadzu IR Pretige-21 Fourier-transformed infrared spectrometer with a DLATGS detector coupled to a 6 mm 3-reflection diamond/Zn-Se crystal ATR plate MIRacle$^{TM}$ (Pike Technologies) and a high pressure clamp. The spectrometer settings were as follows: 4.0 $cm^{-1}$ spectral resolution, 150 scan and using a squared triangular apodisation. Each decalcified and dried sample was placed directly over the ATR plate, and the pressure clamp was applied with the manufacturing default settings. The total area analyzed for each sample varied from 5 to 7 $cm^2$; the analysis of the gross composition of tissues is therefore on the scale of centimeters for the corals.

The pretreatment of spectra was carried out following methods outlined by San-Blas et al. (2011). This included ATR and baseline corrections, scaling between 0 and 1, and the 5-point adjacent averaging second derivative spectrum calculation using the IR Solution Software (Shimadzu). In addition, the atmospheric water and $CO_2$ corrections were confirmed following the procedure reported by Susanne et al. (2006).

### Statistical analysis

Since Fourier-transformed infrared spectroscopy is not quantitative, direct comparison between samples is not possible because the infrared signal intensity for each sample is unique. The best way to avoid this limitation is to use ratios, for 2 samples will be the same when the quotients of 2 or more given points are the same. Thus, we used ratios of IR absorption to compare samples as we assumed that samples were similar when their ratios were equal. To identify the most contrasting variables (i.e. absorption regions), a principal component analysis was performed using standardized data by calculating their standard *z*-scores (i.e. the coordinate of each sample projected over each principal component) as follows:

$$Z_i = \frac{\lambda_i - \bar{\lambda}}{S} \quad (1)$$

where $Z_i$ is the standard score of the sample $(i)$, $\lambda_i$ is the absorbance of second derivate of the sample $(i)$, $\bar{\lambda}$ is the arithmetic mean of values of absorbance of second derivate, and $S$ is the standard deviation of the mean of the absorbance of the second derivate.

The scores for every possible combination of principal components (PCs) were visualized in bivariate scatter plots until the greatest contrast of samples (H, AH, TR and YBD) was achieved. In the present study, the most contrasting PCs were PC1/PC2 and particularly the vector PC1. The amount of variance of each variable explained in a particular PC (i.e. the coefficient or loading of each variable) was also calculated to establish the correlation of an original variable with a PC. The variables with highest and positive loadings ($X_i^+$) had particular values in a set of cases that turned out to be completely different from those of the variables with lower and negative loadings ($X_i^-$). Following this idea, 2 groups of variables were selected: (1) 15 with the highest and positive loadings ($X_i^+$) and (2) 15 with lower and negative loadings ($X_i^-$) for a total of 30 variables with the greatest differences.

The 30 most contrasting variable loadings were sorted from the highest to the lowest and ranked from 1 to 30 according to the highest to smallest loading, respectively. The selected variables were then substituted by the values represented in the second derivative spectral data. A new set of ratios $R_{X_i^+X_i^-}$ was determined using the highest and the lowest values (provided from variables previously ranked as 1 and 30 from above) to calculate the first ratio, the second highest and the second lowest (variables 2 and 29) to calculate the second ratio and so on until the final 15 ratios were calculated for each sample replicate (Eq. 2).

$$R_{X_i^+X_i^-} = \frac{\left(\left|X_i^+\right|\right)}{\left(\left|X_i^+\right| + \left|X_i^-\right|\right)} \qquad (2)$$

The nonparametric Kruskal-Wallis test ($\alpha = 0.05$) was used to contrast the medians of the 15 ratios (i.e. dependent variables) calculated from the second derivate spectral analysis of each sample type. All statistical calculations were carried out using the MVSP software Version 3.11 (Kovach Computing Services).

## RESULTS

### Elucidation of the spectra

Intense and unique absorption bands were observed in the mid-IR region for each sample type (Fig. 2). Lipidic compounds absorb in the region between 2800 and 3000 $cm^{-1}$ because of the asymmetric and symmetric C–H stretching vibrations of the methyl ($-CH_3$) (2956 and 2874 $cm^{-1}$) and methylene ($-CH_2$) radicals (2922 and 2852 $cm^{-1}$; Table 1,

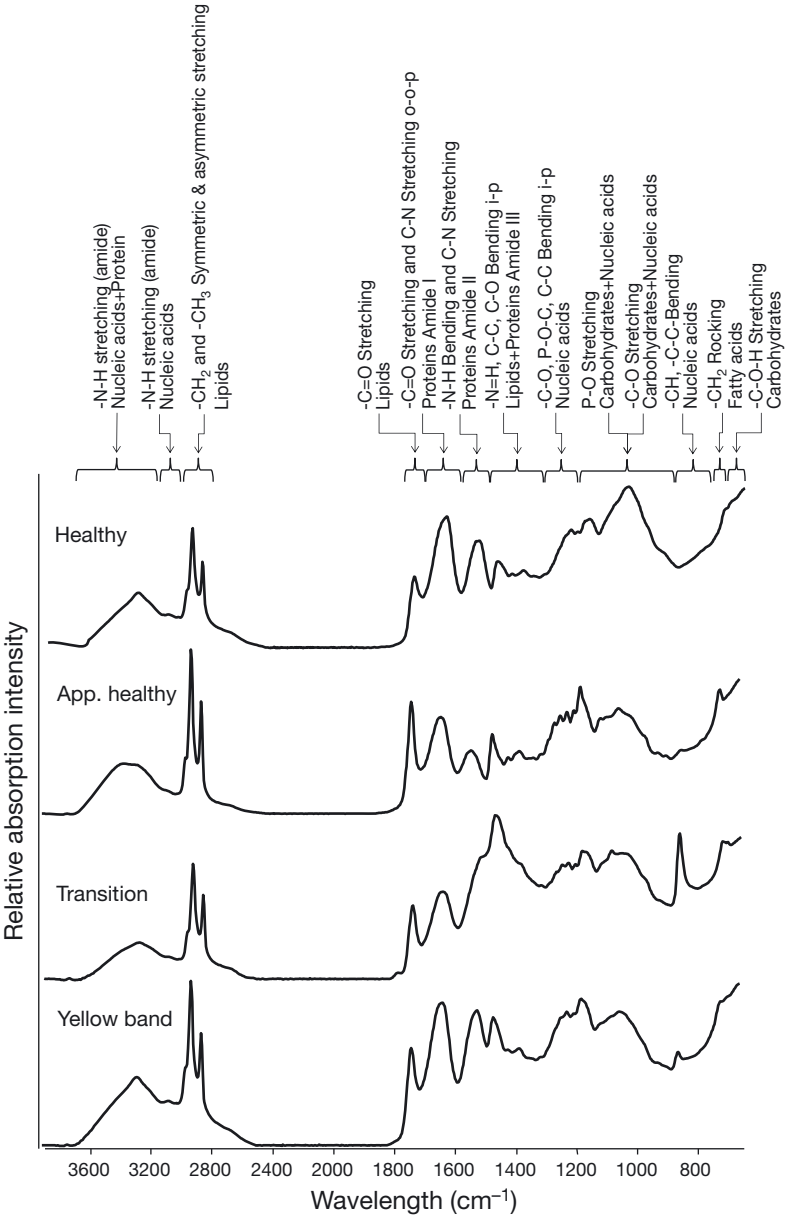


Fig. 2. *Orbicella faveolata*. FITR/ATR elucidation spectra showing the average gross chemical composition for healthy, apparently healthy, transition and yellow band disease tissues

Table 1. *Orbicella faveolata*. FITR/ATR absorption bands of (YBD) yellow band disease, (TR) transition, (AH) apparently healthy and (H) healthy coral tissues. Absorption band description according to Wetzel & LeVine (1999), Miller & Dumas (2006), Farre et al. (2010) and San-Blas et al. (2011)

| YBD | TR | AH | H | Macromolecules associated with each band |
|---|---|---|---|---|
| 3270 | 3270 | 3263 | 3266 | Amide A, N–H stretching, asymmetric stretching |
| 3079 | 3077 | 3079 | 3060 | Amide B, CH trans stretch vibration |
| 3915 | 2915 | 2915 | 2917 | C–H stretching (asymmetric) $CH_2$ |
| 2849 | 2847 | 2847 | 2849 | C–H stretching (symmetric) $CH_2$ |
| | | | | Stretching (symmetric) of $CH_3$ of acyl chains (lipids) |
| 1733 | 1733 | 1731 | 1731 | C–O stretching in saturate esters of triglycerides |
| 1636 | 1634 | 1634 | 1628 | Collagen |
| | | | | Amide I (beta pleated sheet) |
| 1515 | 1515 | 1534 | 1515 | Amide II |
| 1463 | 1461 | 1464 | 1449 | C–H def of $CH_2$ deformation mainly lipids or Amide II |
| 1220 | 1220 | 1220 | 1220 | Collagen $CH_2$ wagging |
| | | | | Nucleic acid |
| | | | | Amide III |
| | | | | PO asymmetric stretching of $PO_2$ |
| 1175 | 1173 | 1175 | 1160 | C–O, C–C stretching, C–O–H, C–O–C deformation of glycogen |
| 1077 | 1077 | 1077 | 1077 | Glycogen and collagen C–N stretching |
| 853 | 853 | 853 | | R–CH $CH_2$ |
| 712 | 710 | 710 | | Vibrations out of the plane of NH |

Fig. 2; Miller & Dumas 2006, Holman et al. 2008). In addition, the band at 1733 to 1736 $cm^{-1}$ arises from ester C–O phosphodiester groups that are present in the lipid compounds, such as triglycerides (Table 1, Fig. 2; Wu et al. 2001). The protein spectrum has 2 primary features: (1) the Amide I (1600 to 1700 $cm^{-1}$) and (2) the Amide II (1500 to 1560 $cm^{-1}$) bands, which arise primarily from the C–O and C–N stretching vibrations of the peptide and protein backbones, respectively (Table 1; Ci et al. 1999, Miller & Dumas 2006, Barth 2007). These features are recorded in the elucidation spectrum of each sample type (Fig. 2).

In addition, the spectra recorded from the 4 types of coral tissue had prominent absorption peaks between 1350 and 1200 $cm^{-1}$, which are mainly linked to the collagen, glycine and proline amino acid sequences (Ami et al. 2004). The bands 1175 and 1160 $cm^{-1}$ can be assigned to the C–O stretching modes of the C–OH groups of certain proteins and C–C, C–O and C–O–C stretching vibration of carbohydrates such as glycogen (Table 1, Fig. 2). The peaks near 1077 and 1220 $cm^{-1}$ are both related to collagen and the symmetric and asymmetric phosphate ($PO_2^{2+}$) stretching modes ($sPO_2^{2+}$ and $asPO_2^{2+}$), respectively. These compounds are not only found in nucleic acids but are also contributors to the asymmetric C–O–C stretching vibration in aliphatic esters and various oligo- and polysaccharides (Neugebauer et al. 2007). The band around 990 $cm^{-1}$ was assigned to a stretching vibration band of the α,α-1,1 linkage characteristic of trehalose (Sakurai et al. 2008), which is an important disaccharide found in many organisms. The band recorded at 960 $cm^{-1}$ was assigned to C–O stretching of the phosphodiester and the ribose C–O deoxyribose, C–C.

The region around 933 $cm^{-1}$ was assigned to wagging vibration of N–H, characteristic of pigments like carotenoids and anthraquinones (Table 1, Fig. 2; Neugebauer et al. 2007). The spectral region below 900 $cm^{-1}$ contains only very poorly resolved spectral features, so an assignment is hard to achieve; however, it is possible to recognize $CH_2$ rocking modes of fatty-acid side chains and the stretching vibration of C–O and C–C bonds of the deoxyribose around 914 $cm^{-1}$ (Neugebauer et al. 2007).

### Comparison of FITR spectra among samples

The chemometric analysis of infrared absorption spectra revealed differences among spectrum profiles, which indicate that the chemical makeup of coral tissues is altered between healthy and YBD states (Fig. 3), suggesting that alterations in the biochemical composition of tissues occur during pathogenesis. The most important variations were recorded at 740, 960, 1180, 1460 and 2852 $cm^{-1}$; all these regions related to chemical bonds of lipids, fatty acids, carbohydrates, proteins or nucleic acids, as described before (Fig. 2). Ratios 693/(693 + 1465 $cm^{-1}$) and 695/(695 + 1463 $cm^{-1}$) significantly decreased (Kruskal-Wallis = 20.1, df = 3, $p < 0.05$) from healthy to YBD tissues, further indicating an increase in the proportion of lipids in relation to carbohydrates and/or a decrease in carbohydrates relative to lipids in YBD, TR and AH tissues compared to healthy corals (Table 2, Fig. 3A,B). A similar trend was recorded for the carbohydrate threalose (Table 2, Fig. 3C). The results also indicate a significant increase (Kruskal-Wallis = 15.8, df = 3, $p < 0.05$) in the ratio 742/(740 + 1183), which indicate that proteins such as collagen

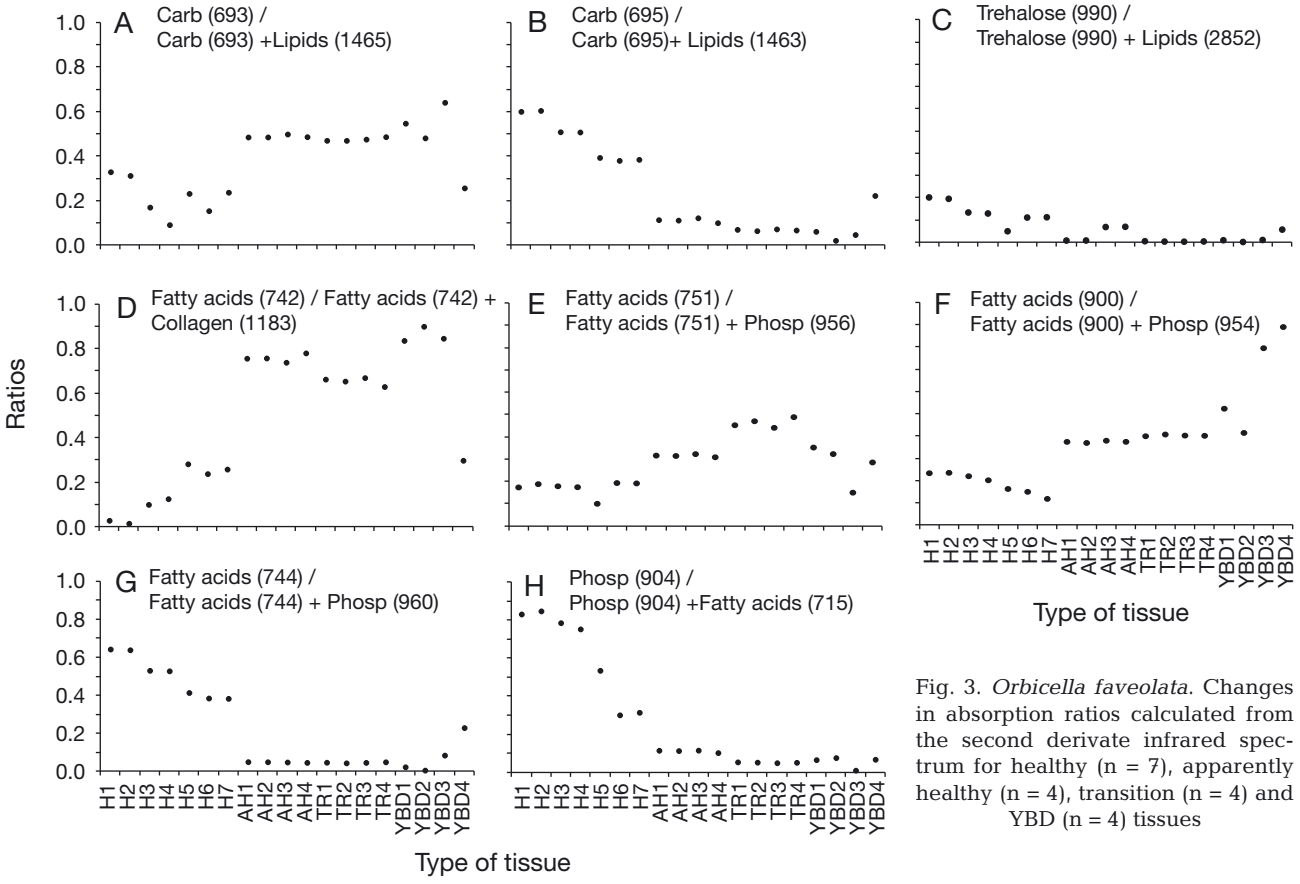


Fig. 3. *Orbicella faveolata*. Changes in absorption ratios calculated from the second derivate infrared spectrum for healthy (n = 7), apparently healthy (n = 4), transition (n = 4) and YBD (n = 4) tissues

Table 2. *Orbicella faveolata*. Mean, standard deviation and p (Kruskal-Wallis test, $\alpha = 0.05$) of ratios from the second derivate of the infrared spectrum of (H) healthy, (AH) apparently healthy, (TR) transition and YBD tissues. Different lowercase letters indicate groups that are significantly different after paired comparisons. *$p < 0.05$

| Ratios | Infrared band assignment | H | | AH | | TR | | YBD | | p |
|---|---|---|---|---|---|---|---|---|---|---|
| | | Mean | SD | Mean | SD | Mean | SD | Mean | SD | |
| 746/(1737+746) | Fatty acids/ (proteins + fatty acids) | 0.05 | 0.039 | 0.081 | 0.0003 | 0.077 | 0.0022 | 0.061 | 0.025 | 0.616 |
| 747/(747+1467) | Carbohydrates/ | 0.235 | 0.199 | 0.101 | 0.0008 | 0.127 | 0.0019 | 0.101 | 0.040 | 0.812 |
| 693/(693+1465) | (carbohydrates + lipid) | 0.504[a] | 0.112 | 0.051[b] | 0.0003 | 0.046[b] | 0.0022 | 0.086[b] | 0.081 | 0.013* |
| 695/(695+1463) | | 0.483[a] | 0.098 | 0.114[b] | 0.0011 | 0.068[b] | 0.0041 | 0.089[b] | 0.071 | 0.011* |
| 740/(740+1461) | Fatty acids/ (fatty acids + carbohydrates) | 0.241 | 0.037 | 0.215 | 0.0006 | 0.218 | 0.0037 | 0.197 | 0.017 | 0.194 |
| 742/(742+1183) | Fatty acids/ (fatty acids + collagen) | 0.151[a] | 0.110 | 0.758[b] | 0.0008 | 0.659b | 0.0062 | 0.721[b] | 0.221 | 0.011* |
| 744/(744+960) | Fatty acids/(fatty acids + | 0.219[a] | 0.085 | 0.486[b] | 0.0001 | 0.471b | 0.0001 | 0.482[b] | 0.126 | 0.023* |
| 749/(749+958) | phospholipids) | 0.266 | 0.103 | 0.377 | 0.0026 | 0.367 | 0.0023 | 0.433 | 0.132 | 0.062 |
| 751/(751+956) | | 0.190[a] | 0.045 | 0.373[b] | 0.0034 | 0.405[b] | 0.0054 | 0.657[b] | 0.216 | 0.006* |
| 900/(900+954) | | 0.171[a] | 0.032 | 0.315[b] | 0.0012 | 0.462[b] | 0.0126 | 0.278[b] | 0.117 | 0.037* |
| 902/(900+952) | | 0.213 | 0.021 | 0.873 | 0.0001 | 0.738 | 0.0614 | 0.499 | 0.370 | 0.164 |
| 904/(904+715) | Phospholipids/(phospho- lipids + fatty acids) | 0.623[a] | 0.239 | 0.114[b] | 0.0011 | 0.052[b] | 0.0009 | 0.054[b] | 0.023 | 0.008* |
| 935/(935+2856) | Carbohydrates/ | 0.111 | 0.065 | 0.161 | 0.0012 | 0.163 | 0.0083 | 0.131 | 0.019 | 0.33 |
| 936/(936+2854) | (carbohydrates + lipid) | 0.072 | 0.032 | 0.098 | 0.0005 | 0.103 | 0.0041 | 0.085 | 0.010 | 0.186 |
| 990/(990+2852) | Trehalose/(trehalose + lipids) | 0.133[a] | 0.052 | 0.007[b] | 0.0001 | 0.003[b] | 0.0011 | 0.019[b] | 0.021 | 0.015* |

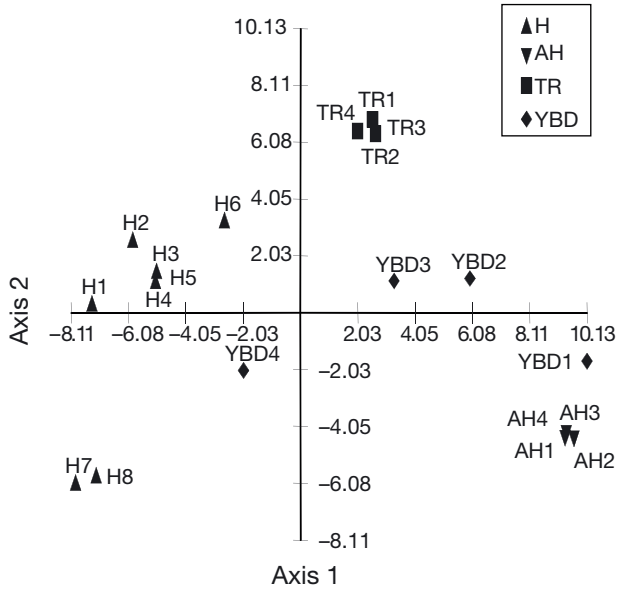


Fig. 4. Principal component analysis showing score plots calculated from the second derivative FTIR spectra (1400 to 2860 $cm^{-1}$). H: healthy; AH: apparently healthy; TR: transition; YBD: yellow band disease tissues

decreased from healthy to YBD tissues in relation to fatty acids absorbing at 742 $cm^{-1}$ (Table 2, Fig. 3D). Furthermore, significant changes of the ratios 744/(742 + 960 $cm^{-1}$), 751/(751 + 956 $cm^{-1}$) and 900/(900 + 954 $cm^{-1}$) indicate a relative decrease in phospholipids as well as an increase in fatty acids in YBD, AH and TR coral tissues compared to healthy corals (Table 2, Fig. 3D,E,F). Thus, the analysis of the infrared spectrum indicates that TR and YBD tissues separate from H ones, and AH tissues are more similar to TR and YBD tissues in terms of their bulk molecular composition (Fig. 4).

## DISCUSSION

In the present study, we utilized analytic techniques and chemometric methods widely used to determine the gross molecular composition of plant and animal tissues to compare healthy, apparently healthy, transition and YBD tissues in the reef-building coral *Orbicella faveolata*. The results showed that each sample type has a different fingerprint infrared spectrum, which indicates that the gross molecular composition of coral tissues varied from healthy to YBD tissues. Major changes occurred in the spectrum of molecules that constitute proteins, carbohydrates and phospholipids in YBD-afflicted corals. While the concentration of these compounds in each of the different types of tissues analyzed remains unknown, we showed that the shape of infrared emissions of healthy tissues is different than that of YBD tissues. We believe that Fourier-transformed infrared spectroscopy is an excellent tool to get molecular fingerprints of healthy corals and an easy way to visualize departures from this healthy condition in terms of the bulk chemical composition of the sample. This technique along with analytic procedures can be used as a powerful tool of early diagnosis of healthy corals and also for detecting families of compounds susceptible to change during pathogenesis. Changes in infrared absorption in the regions assigned to molecules that constitute carbohydrate bonds might be explained by a disruption of the mutualistic association between zooxanthellae and their coral hosts from healthy to YBD tissues. It is believed that photosynthetic performance in YBD tissues is compromised as the concentration of photosynthetic pigments, the density of zooxanthellae and the mitotic index of zooxanthellae are significantly lower than in normal tissues (Cervino et al. 2001, 2004). Zooxanthellae photosynthesize while residing inside the corals, continuously transferring to them up to 95% of their photosynthetic products (Muscatine 1990). These microalgae provide to the corals a variety of nutritional requirements for tasks such as maintenance, synthesis of new cells, skeletal matrix and mucus, deposition of calcium carbonate and the storage of energy-rich compounds for coral reproduction (Muscatine & Cernichiari 1969, Crossland et al. 1980a,b, Muscatine et al. 1981, 1984, Kellogg & Patton 1983, Rinkevich & Loya 1983, 1984, Stimson 1987, Rinkevich 1989). When the coral loses its zooxanthellae, it loses its main energy resource, risking its essential biological functions (Hoegh-Guldberg 1999, Wilkinson 1999, 2000). Reduced proteins and lipids (Porter et al. 1989, Michalek-Wagner & Willis 2001), lowered growth rate (Goreau & Macfarlane 1990), lowered calcification and repair capabilities (Meesters & Bak 1993) and termination of gametogenesis (Szmant & Gassman 1990, Ward 2000, Fine et al. 2001) have all been reported following reduction in zooxanthellae densities. We have found evidence of molecular variations that were principally associated with changes in lipids, fatty acids, carbohydrates and protein signals (Figs. 2 & 3), all of them directly or indirectly related to photosynthetic performance.

The observed increase in the absorption of the infrared band associated with molecules that constitute lipids in YBD tissues could be associated with the active transport of photosynthates from H and/or

AH tissues to the lesions. An important consequence of modularity may be the ability to reprioritize pathways of resource transport among the units of a colony in response to various stresses caused by biotic and abiotic factors. In corals, the transport and translocation of organic compounds to regions of greater demand is well documented (Pearse & Muscatine 1971, Taylor 1977, Muscatine et al. 1981, Muscatine 1990). During tissue regeneration, intra-colonial transport of $^{14}C$-labeled compounds has been demonstrated for many coral species (Oren et al. 1997, 1998). These studies indicated that the products required for lesion recovery are supplied not only by polyps directly bordering the injured area but also by polyps located farther away (up to 10 cm from the injured area) and that the extent of this translocation is regulated by the size and shape of the injury. The results of the present study appear to suggest that translocation of energy-rich compounds such as lipids might occur to heal YBD tissues, whereas the decrease of carbohydrates and proteins in YBD and TR tissues could be the result of reduced photosynthesis in YBD tissues and/ or the rapid depletion of these compounds associated with repairing processes.

The translocation of photosynthates occurs not only from coral tissues but also from endolithic algae that associate with coral skeletons. This is particularly important in bleached corals, as transparent tissues allow more light to reach the coral skeleton, enhancing endolithic algal growth (Fine et al. 2004). Fine & Loya (2002) argued that this alternative source of energy may be vital for the survivorship of bleached corals, allowing gradual recruitment of zooxanthellae and subsequent recovery during the following winter. Lesions of YBD are similar to pale and/or bleached corals; therefore, endolithic algae might play an important role in transferring photoassimilates to YBD lesions and might explain why the mortality associated with YBD tissues is slow (i.e. cm $mo^{-1}$; Bruckner & Bruckner 2006) compared to other diseases such as white plague (i.e. cm $d^{-1}$; Weil 2004).

The translocation of photoassimilates in fact occurs in diseased corals. Recently, Roff et al. (2006) investigated the production and translocation of photoassimilates towards white syndrome lesions (WSLs) and artificially inflicted lesions in healthy and diseased colonies of tabular *Acropora* spp. They found that photoassimilates were preferentially orientated away from active WSLs, with minimal translocation observed in the lesion borders, whilst artificial lesions had an active translocation of photoassimilates for tissue regeneration. They also reported that transport of photoassimilates in healthy coral colonies was preferentially oriented toward artificial lesions with a higher perimeter–area ratio, although translocation towards WSL boundaries was minimal even though the lesion perimeter was often the width of the colony (>200 cm).

YBD is known to affect *Orbicella faveolata* in various ways: (1) altering the structural integrity of coral tissues and their zooxanthellae (Cervino et al. 2001, 2004), (2) affecting antimicrobial and lysozyme-like activities of the coral host (Mydlarz et al. 2009), (3) reducing the fecundity of coral polyps located within YBD lesions and the interface between apparently healthy and diseased tissues (Weil et al. 2009) and (4) producing structural (Cróquer et al. 2012) and functional (Kimes et al. 2010) phase shifts in the microbial communities associated with healthy corals. The latter is particularly important because bacterial assemblages associated with corals are capable of using different carbon sources, photosynthates and organic and inorganic compounds present in the polysaccharide mucus layer of corals and the coral tissues (Ritchie & Smith 2004). Phase shifts in bacterial communities may, therefore, change the chemical composition of both the coral mucus and the coral tissues. Thus, it should not be surprising that all these pathological changes are accompanied by significant alteration of the gross chemical composition of coral tissues affected by YBD.

In conclusion, Fourier-transformed mid-infrared spectroscopy revealed significant differences in the chemical composition between healthy and YBD tissues. The mechanisms that explain this pattern remain uncertain; thus, future studies should focus on testing the role of translocation of photoassimilates from H tissues and/or from endolithic algae to YBD tissues and identifying the importance of functional and structural microbial shifts in determining these changes. The present study opens a promising field of research that must be complemented with analytic methods aimed to determine the actual concentration of chemical compounds such as lipids, carbohydrates and proteins that might be susceptible to change during pathogenesis.

*Acknowledgements*. This project was partially funded by the Decanato de Investigaciones, Universidad Simón Bolívar. We thank INTECMAR (Instituto de Tecnologías y Ciencias Marinas) for providing logistic support; and 3 anonymous reviewers for their comments, which improved the quality of the manuscript.

LITERATURE CITED


Ami D, Natalello A, Zullini A, Doglia SM (2004) Fourier transform infrared micro spectroscopy as a new tool for nematode studies. FEBS Lett 576:297–300

Bachali S, Jager M, Hassanin A, Schoentgen F, Jollès P, Fiala-Medioni A, Deutsch JS (2002) Phylogenetic analysis of invertebrate lysozymes and the evolution of lysozyme function. J Mol Evol 54:652–664

Barth A (2007) Infrared spectroscopy of proteins. Biochim Biophys Acta 1767:1073–1101

Bruckner AW, Bruckner RJ (2006) Consequences of yellow band disease (YBD) on *Montastraea annularis* (species complex) populations on remote reefs off Mona Island, Puerto Rico. Dis Aquat Org 69:67–73

Bruun SW, Kohler A, Adt I, Sockalingum GD, Manfait M, Martens H (2006) Correcting attenuated total reflection–Fourier transform infrared spectra for water vapor and carbon dioxide. Appl Spectrosc 60:1029–1039

Cervino J, Goreau TJ, Nagelkerken I, Smith GW, Hayes R (2001) Yellow band and dark spot syndromes in Caribbean corals: distribution, rate of spread, cytology, and effects on abundance and division rate of zooxanthellae. Hydrobiologia 460:53–63

Cervino JM, Hayes RL, Polson SW, Polson SC, Goreau TJ, Martinez RJ, Smith GW (2004) Relationship of *Vibrio* species infection and elevated temperatures to yellow blotch/band disease in Caribbean corals. Appl Environ Microbiol 70:6855–6864

Chimetto LA, Brocchi M, Thompson CC, Martins RCR, Ramos HR, Thompson FL (2008) Vibrios dominate as culturable nitrogen-fixing bacteria of the Brazilian coral *Mussismilia hispida*. Syst Appl Microbiol 31:312–319

Ci XY, Gao YT, Feng J, Guo ZQ (1999) Fourier transform infrared spectroscopic characterization of human breast tissue: implications for breast cancer diagnosis. Appl Spectrosc 53:257–371

Cortés J (2003) Latin American coral reefs, 1st edn. Elsevier, Amsterdam

Cróquer A, Bastidas C, Elliott E, Sweet M (2012) Bacterial assemblages shifts from healthy to yellow band states in the dominant reef coral *Montastraea faveolata*. Environ Microbiol Rep 5:90–96

Crossland CJ, Barnes DJ, Borowitzka MA (1980a) Diurnal lipid and mucus production in the staghorn coral *Acropora acuminata.* Mar Biol 60:81–90

Crossland CJ, Barnes DJ, Cox T, Devereux M (1980b) Compartmentation and turnover of organic carbon in the staghorn coral *Acropora formosa.* Mar Biol 59:181–187

Farre B, Cuif JP, Dauphin Y (2010) Occurrence and diversity of lipids in modern coral skeletons. Zoology 113: 250–257

Ferrier-Pagès C, Gattuso JP, Cauwet G, Jaubert J, Allemand D (1998) Release of dissolved organic carbon and nitrogen by the zooxanthellate coral *Galaxea fascicularis.* Mar Ecol Prog Ser 172:265–274

Ferrier-Pagès C, Leclercq N, Jaubert J, Pelegri SP (2000) Enhancement of pico- and nanoplankton growth by coral exudates. Aquat Microb Ecol 21:203–209

Fine M, Loya Y (2002) Endolithic algae: an alternative source of photoassimilates during coral bleaching. Proc R Soc Lond B 269:1205–1210

Fine M, Zibrowius H, Loya Y (2001) *Oculina patagonica*: a non-lessepsian scleractinian coral invading the Mediterranean Sea. Mar Biol 138:1195–1203

Fine M, Steindler L, Loya Y (2004) Endolithic algae photoacclimate to increased irradiance during coral bleaching. Mar Freshw Res 55:115–121

Gochfeld DJ, Aeby GS (2008) Antibacterial chemical defenses in Hawaiian corals provide possible protection from disease. Mar Ecol Prog Ser 362:119–128

Goreau TJ, Macfarlane AH (1990) Reduced growth rate of *Montastrea annularis* following the 1987–1988 coral bleaching event. Coral Reefs 8:211–215

Green EP, Bruckner AW (2000) The significance of coral disease epizootiology for coral reef conservation. Biol Conserv 96:347–361

Hoegh-Guldberg O (1999) Climate change, coral bleaching and the future of the world's coral reefs. Mar Freshw Res 50:839–866

Holman HYN, Bjornstad KA, Martin MC, Mckinney WR, Blakely EA, Blankenberg FG (2008) Mid-infrared reflectivity of experimental atheromas. J Biomed Opt 13: 030503

Kellogg RB, Patton JS (1983) Lipid droplets, medium of energy exchange in the symbiotic anemone, *Condylactis gigantea*, a model coral polyp. Mar Biol 75:137–149

Kelman D, Kashman Y, Rosenberg E, Kushmaru A, Loya Y (2006) Antimicrobial activity of red-sea corals. Mar Biol 149:357–363

Kimes NE, Van Nostrand JD, Weil E, Zhou JZ, Morris PJ (2010) Microbial functional structure of *Montastraea faveolata*, an important Caribbean reef-building coral, differs between healthy and yellow-band diseased colonies. Environ Microbiol 12:541–556

Kvennefors ECE, Sampayo E, Ridgway T, Barnes AC, Hoegh-Guldberg O (2010) Bacterial communities of two ubiquitous Great Barrier Reef corals reveals both site and species-specificity of common bacterial associates. PLoS ONE 5:e10401

Lesser M, Bythell JC, Gates RD, Johnston RW, Hoegh-Guldberg O (2007) Are infectious diseases really killing corals? Alternative explanations of experimental and ecological data. J Exp Mar Biol Ecol 346:36–44

Meesters EH, Bak RPM (1993) Effects of coral bleaching on tissue regeneration potential and colony survival. Mar Ecol Prog Ser 96:189–198

Michalek-Wagner K, Willis BL (2001) Impact of bleaching on the soft coral *Lobophytum compactum*. II. Biochemical changes in adults and their eggs. Coral Reefs 19:240–246

Miller LM, Dumas P (2006) Chemical imaging of biological tissue with synchrotron infrared light. Biochim Biophys Acta 1758: 846–857

Muscatine L (1990) The role of symbiotic algae in carbon and energy flux in reef corals. Coral Reefs 25:1–29

Muscatine L, Cernichiari E (1969) Assimilation of photosynthetic products of zooxanthellae by a reef coral. Biol Bull 137:506–523

Muscatine L, McCloskey LR, Marian RF (1981) Estimating the daily contribution of carbon from zooxanthellae to coral animal respiration. Limnol Oceanogr 26:601–611

Muscatine L, Falkowski PG, Porter JW, Dubinsky Z (1984) Fate of photosynthetically fixed carbon in light- and shade-adapted colonies of the symbiotic coral *Stylophora pistillata.* Proc R Soc Lond B Biol Sci 222:181–202

Mydlarz LD, Couch CS, Weil E, Smith G, Harvell CD (2009) Immune defenses of healthy, bleached and diseased *Montastraea faveolata* during a natural bleaching event. Dis Aquat Org 87:67–78

Neugebauer U, Schmid U, Baumann K, Ziebuhr W, Kozit-

skaya S, Deckert V, Schmitt M (2007) Towards a detailed understanding of bacterial metabolism — spectroscopic characterization of *Staphylococcus epidermidis*. ChemPhysChem 8:124–137

Nissimov J, Rosenberg E, Munn CB (2009) Antimicrobial properties of resident coral mucus bacteria of *Oculina patagonica*. FEMS Microbiol Lett 292:210–215

Olson ND, Ainsworth TD, Gates RD, Takabayashi M (2009) Diazotrophic bacteria associated with Hawaiian *Montipora* corals: diversity and abundance in correlation with symbiotic dinoflagellates. J Exp Mar Biol Ecol 371: 140–146

Oren U, Rinkevich B, Loya Y (1997) Oriented intra-colonial transport of $^{14}C$ labeled materials during coral regeneration. Mar Ecol Prog Ser 161:117–122

Oren U, Brickner I, Loya Y (1998) Prudent sessile feeding by the corallivore snail *Coralliophila violacea* on coral energy sinks. Proc R Soc Lond B Biol Sci 265:2043–2050

Pearse VB, Muscatine L (1971) Role of symbiotic algae (zooxanthellae) in coral calcification. Biol Bull 141:350–363

Porter JW, Fitt WK, Spero HJ, Rogers CS (1989) Bleaching in reef corals: physiological and stable isotopic responses. Proc Natl Acad Sci USA 86:9342–9346

Raina JB, Tapiolas D, Willis BL, Bourne DG (2009) Coral-associated bacteria and their role in the biogeochemical cycling of sulfur. Appl Environ Microbiol 75:3492–3501

Rinkevich B (1989) The contribution of photosynthetic products to coral reproduction. Mar Biol 101:259–263

Rinkevich B, Loya Y (1983) Short-term fate of photosynthetic products in a hermatypic coral. J Exp Mar Biol Ecol 73: 175–184

Rinkevich B, Loya Y (1984) Coral illumination through an optic glass-fiber: incorporation of $^{14}C$ photosynthates. Mar Biol 80:7–15

Ritchie KB (2006) Regulation of microbial populations by coral surface mucus and mucus-associated bacteria. Mar Ecol Prog Ser 322:1–14

Ritchie KB, Smith GW (1995) Preferential carbon utilization by surface bacterial communities from water mass, normal, and white-band diseased *Acropora cervicornis*. Mol Mar Biol Biotechnol 4:345–352

Ritchie KB, Smith GW (2004) Microbial communities of coral surface mucopolysaccharide layers. In: Rosenberg E, Loya Y (eds) Coral health and disease. Springer, Berlin, p 259–264

Roff G, Fine M, Hoegh-Gulberg O (2006) Intra-colony response to Acroporid 'white syndrome' lesions in tubular *Acropora* spp. (Scleractinea). Coral Reefs 25:255–264

Rohwer F, Kelley S (2004) Culture-independent analyses of coral-associated microbes. In: Rosenberg E, Loya Y (eds) Coral health and disease. Springer, Berlin, p 265–277

Rowan R (1998) Diversity and ecology of zooxanthellae on coral reefs. J Phycol 34:407–417

Rowan R, Knowlton N, Baker A, Jara J (1997) Landscape ecology of algal symbionts creates variation in episodes of coral bleaching. Nature 388:265–269

Sakurai M, Furuki T, Akao KI, Tanaka D and others (2008) Vitrification is essential for anhydrobiosis in an African chironomid, *Polypedilum vanderplanki*. Proc Natl Acad Sci USA 105:5093–5098

San-Blas E, Guerra M, Portillo E, Esteves I, Cubillán N, Alvarado Y (2011) ATR/FTIR characterization of *Steinernema glaseri* and *Heterorhabditis indica*. Vibr Spectroscopy 57:220–228

Shnit-Orland M, Kushmaro A (2009) Coral mucus-associated bacteria: a possible first line of defence. FEMS Microbiol Ecol 67:371–380

Stimson JS (1987) Location, quantity and rate of change in quantity of lipids in tissue of Hawaiian hermatypic corals. Bull Mar Sci 41:889–904

Sutherland KP, Porter JW, Torres C (2004) Disease and immunity in Caribbean and Indo-Pacific zooxanthellate corals. Mar Ecol Prog Ser 266:273–302

Sweet MJ, Croquer A, Bythell JC (2011a) Dynamics of bacterial community development in the reef coral *Acropora muricata* following experimental antibiotic treatment. Coral Reefs 30:1121–1133

Sweet MJ, Croquer A, Bythell JC (2011b) Bacterial assemblages differ between compartments within the coral holobiont. Coral Reefs 30:39–52

Szmant A, Gassman NJ (1990) The effect of prolonged 'bleaching' on the tissue biomass and reproduction of the reef coral *Montastrea annularis*. Coral Reefs 8:217–224

Taylor DL (1977) Intra-colonial transport of organic compounds and calcium in some Atlantic reef corals. In: Taylor DL (ed) Proc 3rd Int Coral Reef Symp. Rosenstiel School of Marine and Atmospheric Science, University of Miami, Miami, FL, p 431–436

Ward S (2000) Changes in coral reproduction following slight changes in temperature and bleaching. In: Okamoto M (ed) Proc JAMSTEC Int Coral Reef Symp: coral reef biodiversity and health as indicators of environmental change, February 2000. Science and Technology Agency, Tokyo, p 94–111

Wegley L, Yu YN, Breitbart M, Casas V, Kline DI, Rohwer F (2004) Coral-associated Archaea. Mar Ecol Prog Ser 273: 89–96

Weil E (2004) Coral reef diseases in the wider Caribbean. In: Rosenberg E, Loya Y (eds) Coral health and disease. Springer-Verlag, New York, NY, p 35–68

Weil E, Smith G, Gil-Agudelo DL (2006) Status and progress in coral reef disease research. Dis Aquat Org 69:1–7

Weil E, Cróquer A, Urreiztieta I (2009) Yellow band disease compromises the reproductive output of the reef-building coral *Montastraea faveolata* (Anthozoa, Scleractinia). Dis Aquat Org 87:45–55

Wetzel DL, LeVine SM (1999) Imaging molecular chemistry with infrared microscopy. Science 285:1224–1225

Wilkinson CR (1999) The 1997–1998 mass bleaching event around the world. Compilation of Internet reports, global reef monitoring network. Australian Institute of Marine Science, Townsville

Wilkinson CR (ed) (2000) Status of coral reefs of the world. (2000) Australian Institute of Marine Science, Townsville

Wu JG, Xu YZ, Sun CW, Soloway RD and others (2001) Distinguishing malignant from normal oral tissues using FTIR fiber-optics techniques. Biopolymers 62: 185–192

*Editorial responsibility: Garriet Smith, Aiken, South Carolina, USA*

*Submitted: June 3, 2013; Accepted: October 1, 2013*
*Proofs received from author(s): December 19, 2013*